Gamma-ray astronomy / Astronomie des rayons gamma – Volume 2

Gamma-ray bursts at high and very high energies

Les sursauts gamma à haute et très haute énergie

Frédéric Piron

LUPM, CC 72, CNRS/IN2P3, Université de Montpellier, place Eugène-Bataillon, 34095 Montpellier cedex 05, France

A R T I C L E   I N F O

A B S T R A C T

Gamma-Ray Bursts (GRBs) are extra-galactic and extremely energetic transient emissions of gamma rays, which are thought to be associated with the death of massive stars or the merger of compact objects in binary systems. Their huge luminosities involve the presence of a newborn stellar-mass black hole emitting a relativistic collimated outflow, which accelerates particles and produces non-thermal emissions from the radio domain to the highest energies. In this article, I review recent progresses in the understanding of GRB jet physics above 100 MeV, based on Fermi observations of bright GRBs. I discuss the physical implications of these observations and their impact on GRB modeling, and I present some prospects for GRB observation at very high energies in the near future.

© 2016 Académie des sciences. Published by Elsevier Masson SAS. This is an open access article under the CC BY-NC-ND license (http://creativecommons.org/licenses/by-nc-nd/4.0/).

R É S U M É

Les sursauts gamma sont des phénomènes explosifs extrêmement énergétiques et des émissions transitoires de rayonnement gamma d'origine extra-galactique. Ils sont associés à la fin de vie d'étoiles massives ou à la fusion d'objets compacts d'un même système binaire. Leur grande luminosité implique la présence d'un trou noir de masse stellaire nouvellement formé émettant un écoulement relativiste collimaté qui accélère les particules et produit une émission non thermique du domaine radio jusqu'aux plus hautes énergies. Dans cet article, je passe en revue les progrès récents dans la compréhension de la physique des jets de sursauts gamma au-dessus de 100 MeV, sur la base d'observations de sursauts brillants avec Fermi. Je discute les implications physiques immédiates de ces observations et leurs conséquences sur la modélisation, et je présente les perspectives pour l'observation de sursauts gamma aux très hautes énergies dans les années à venir.

© 2016 Académie des sciences. Published by Elsevier Masson SAS. This is an open access article under the CC BY-NC-ND license (http://creativecommons.org/licenses/by-nc-nd/4.0/).
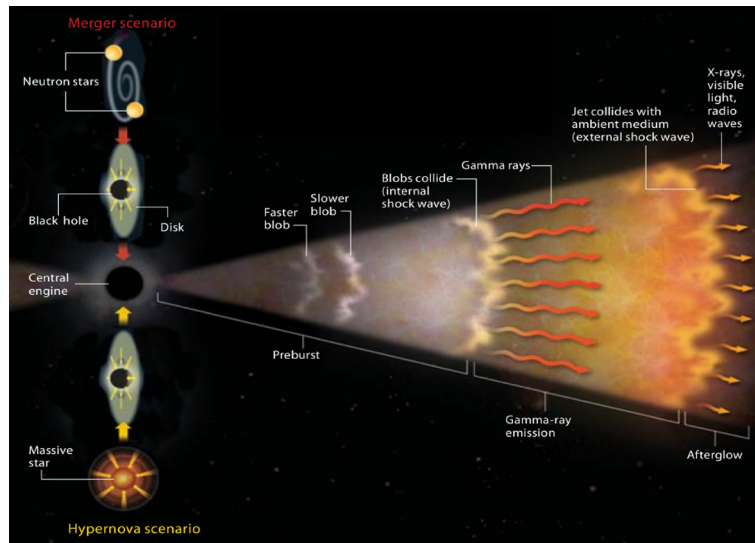
Fig. 1. Illustration of the internal/external shock scenario for gamma-ray bursts (credit NASA).

1. Introduction

Gamma-Ray Bursts (GRBs) are powerful high-energy transient emissions from sources at cosmological distances. They appear randomly on the celestial sphere, and they are characterized by a short phase of intense and erratic emission in hard X rays and gamma rays, lasting from few milliseconds to hundreds of seconds. Following this so-called prompt phase, GRBs exhibit a long-lasting activity (the afterglow phase) where the observed flux decreases rapidly in time, with an emission peak energy shifting to longer wavelengths (X rays, visible and radio) on time scales spanning from hours to weeks.

Assuming that GRBs radiate isotropically, their energy release in X rays and gamma rays (typically $\sim 10^{44-47}$ J $= 10^{51-54}$ erg) exceeds hundred times the total energy radiated by a supernova ($\sim 10^{42}$ J $= 10^{49}$ erg). The widely accepted scenario [1–3] which is invoked to explain GRB huge luminosities involves a newborn stellar-mass black hole emitting a relativistic collimated outflow (Fig. 1). The GRB progenitors as well as the physical conditions which are required to produce and accelerate the relativistic jet are nevertheless still unclear. The distribution of GRB duration was found to be bimodal [4,5], revealing the existence of two distinct populations. Long GRBs (i.e. with typical prompt emission durations $\gtrsim 2$ s) are believed to be produced by the collapse of fast rotating massive stars ($\gtrsim 30\, M_\odot$, of Wolf–Rayet type), as suggested by their association with nearby core-collapsed supernovae of types Ib/Ic. Short GRB progenitors are more elusive and may be connected to the merging of two compact objects in binary systems (two neutron stars or a neutron star and a stellar-mass black hole). The new generation of gravitational wave detectors such as Advanced Virgo/LIGO[1] should be able to detect the corresponding emission from short GRBs, and to help shed light on their progenitors in the coming years [6].

The highly variable gamma-ray emission characteristic of the GRB prompt phase is associated with the dissipation of the jet internal energy in mildly relativistic shocks taking place at a distance $R \approx 10^{12-13}$ m from the central engine, where particles are accelerated and emit non-thermal radiations. The properties of the jet (speed, structure, collimation, composition, energy reservoirs, magnetization, emission sites) as well as the micro-physics (energy dissipation mechanisms, shock acceleration efficiency, radiation processes and internal opacity effects, role of magnetic fields, etc.) are not precisely known. The afterglow phase is associated with the jet deceleration at a distance $R \approx 10^{14-15}$ m from the central engine, where an external shock is formed by the interaction of the jet with the circum-burst medium. This relativistic forward shock accelerates electrons which radiate synchrotron emission observed from the radio to the gamma-ray domain.

The study of acceleration and emission processes in GRB jets requires well-sampled (both spectrally and temporally) multi-wavelength observations of objects with measured redshifts. Significant progress has been made possible thanks to the space missions Fermi (launched in 2008) and Swift (launched in 2004).[2] Following a previous contribution to *Comptes Rendus Physique* on Fermi results [8], this article focuses on GRB physics[3] above 100 MeV ("high energies" hereafter) up to the very high-energy gamma-ray domain (above 100 GeV). In section 2, I briefly review some of the few GRB detections at

---

[1] https://wwwcascina.virgo.infn.it/advirgo, https://www.advancedligo.mit.edu.

[2] Detailed reviews can be found elsewhere, e.g., in [7].

[3] The detection of high-energy photons from distant GRBs is also a powerful tool for non-GRB science. Specifically, they have been used to probe the quantum-gravitational nature of space-time and to test the existence of Lorentz Invariance Violation (LIV) as a consequence of some Quantum Gravity theories. In addition, gamma rays with energies above ~ 10 GeV can be absorbed by the Extra-galactic Background Light (EBL) when traveling from the emitting region to the observer, providing useful constraints on this cosmic diffuse radiation field, which results from the emission of the first stars and its subsequent reprocessing by dust in the inter-stellar medium. Both topics (LIV and EBL) are addressed in detail in another article in this volume [9].
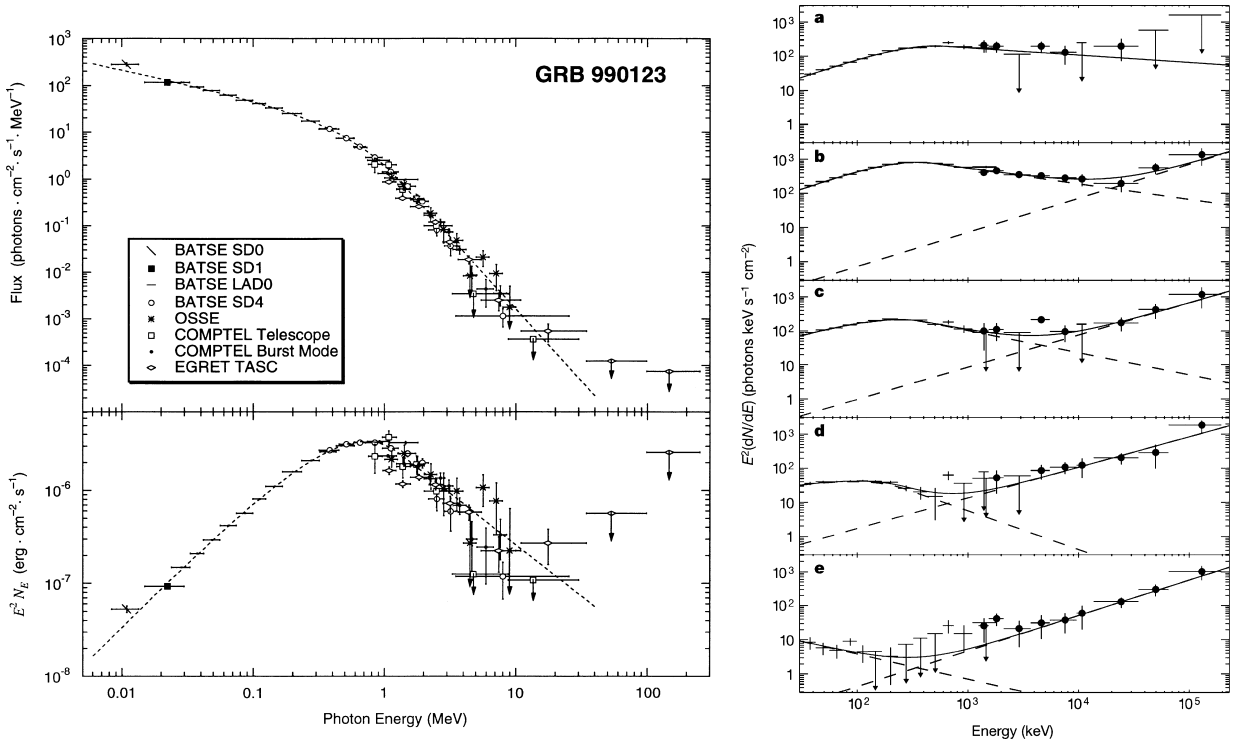
Fig. 2. Left: GRB 990123 photon spectrum (top panel) and spectral energy distribution (bottom panel, in $\mathrm{erg\,cm^{-2}\,s^{-1}} = 10^{-3}\,\mathrm{W\,m^{-2}}$) as measured by the four instruments onboard the Compton Gamma-Ray Observatory [11]. Right: GRB 941017 spectral energy distributions as measured by the CGRO/BATSE and the CGRO/EGRET between -18 s and $+211$ s (from top to bottom) [12].

high energies before the Fermi era, and the questions they raised. Fermi observations of GRBs have greatly improved the detection statistics, and they constitute the best set of high-energy data so far. In section 3, I recall the main findings from this mission, including notable GRBs as well as population studies, and I present the common properties in GRB temporal and spectral behavior at high energies. Section 4 addresses the physical implications of these observations and their impact on GRB modeling. In section 5, I discuss the prospects for GRB observation at very high energies with the new generation of ground-based Cherenkov telescopes in the coming years, before concluding in section 6.

2. GRBs at high energies before the Fermi era

Before the advent of Fermi, non-thermal spectra in the prompt phase were usually represented in the keV–MeV energy range by the phenomenological Band function [10], which is composed of two smoothly-connected power laws with respective indices α and β (Fig. 2, left):

$$\frac{dN}{dE}(E|N_0, E_{\mathrm{p}}, \alpha, \beta) = N_0 \begin{cases} E^{\alpha} \exp[-E(2+\alpha)/E_{\mathrm{p}}], & E \leq E_{\mathrm{p}}\frac{\alpha-\beta}{2+\alpha} \\[2ex] E^{\beta}\left[E_{\mathrm{p}}\frac{\alpha-\beta}{2+\alpha}\right]^{(\alpha-\beta)}\exp[\beta-\alpha], & E > E_{\mathrm{p}}\frac{\alpha-\beta}{2+\alpha} \end{cases} \tag{1}$$

where $\frac{dN}{dE}$ is the photon spectrum[4] (in $\mathrm{m^{-2}\,s^{-1}\,keV^{-1}}$) and E_{p} is the peak energy of the spectral energy distribution $E^2\frac{dN}{dE}$, ranging from a few hundreds of keV to a few MeV. At higher energies, some GRB emission has been detected in a few distinct cases with the Energetic Gamma-Ray Experiment Telescope (EGRET, 30 MeV–30 GeV) onboard the Compton Gamma-Ray Observatory (CGRO, 1991–2000).[5] The high-energy emission from GRB 930131 [14] was consistent with an extrapolation from its keV–MeV spectrum as measured by the CGRO's Burst And Transient Source Experiment (BATSE). In the case of GRB 941017 [12], an additional and hard power law was observed up to 200 MeV without any spectral attenuation (Fig. 2, right). This extra component had a much larger energetics and lasted significantly longer ($\sim$200 s) than the Band

---

[4] In this article, photon indices will be always chosen negative, i.e. $\frac{dN}{dE} \propto E^{\gamma}$ with $\gamma < 0$, following the definition of the Band function.

[5] And in one case (GRB 080514B) by the GRID instrument onboard Astro-rivelatore Gamma a Immagini LEggero (AGILE) [13].

component detected by the CGRO/BATSE at sub-MeV energies. Moreover, both components appeared uncorrelated, the extra component exhibiting a temporal stability that contrasts with the gradual decrease of the Band component intensity and peak energy. Since the Band component is commonly attributed to the synchrotron emission of internal-shock accelerated electrons (see section 4.2), these observations ruled out a possible inverse Compton origin of the extra component, as is for instance expected from simple Synchrotron Self Compton (SSC) models. Alternate interpretations were considered, such as a possible hadronic origin (e.g., gamma-ray emission of secondary particles produced in internal cascades initiated by accelerated protons or ions) or an external shock emission [15]. In the case of GRB 940217 [16], a delayed high-energy emission was observed up to ∼90 min, with an 18 GeV photon detected after ∼75 min. Possible interpretations of these observations included a GRB late activity, a hadronic spectral component, or an SSC emission in the afterglow phase.

These pioneering studies illustrate the diversity in GRB spectral and temporal properties at high energies, which can differ from the main emission spectral component that culminates at a few hundreds of keV. They opened several questions about GRB jet physics, anticipating the advances which were later provided by Fermi:

– What is the nature of the accelerated particles responsible for the high-energy emissions?
– Where and how are these particles accelerated? Within internal or external shocks? What is their spectrum?
– When do internal shocks end (prompt phase) and external shocks start (afterglow phase)?
– What are the dominant radiative processes at high energies? At which distance/radius from the central engine are non-thermal emissions produced?
– Is the extra spectral component common to most GRBs?
– What is the maximum detectable energy and what is the shape of the spectral attenuation at the highest energies? Does it mark the end of the particle spectrum, is it caused by a lower radiation efficiency or by opacity effects within the source?

Precious information on the gamma-ray opacity to pair production ($\gamma + \gamma \rightarrow e^+ + e^-$) is provided by the detection of high-energy photons, which imply strong evidence for relativistic outflows as the sites of GRB prompt emission. Together with GRB variability and brightness at high energies, these photons can be used to set strong limits on the jet bulk Lorentz factor Γ. For a source at rest, the short variability time scale t_v observed in the prompt light curves gives a limit on the size of the emitting zone $R < c\, t_v$, based on a simple causality argument. Combined with the large luminosities $L_{iso} \sim 10^{43-46}$ W (10^{50-53} erg s^{-1}) inferred by assuming an isotropic emission, this compactness would be sufficient for gamma rays of energy E to annihilate in pairs with dense fields of softer photons. Since pair production is most efficient for soft target photons of energies $\epsilon \simeq m_e^2 c^4 / E$, the implied optical depth is:

$$\begin{aligned}
\tau_{\gamma\gamma}(E) &\simeq \sigma_T\, n_{ph}(\epsilon)\, R \\
&= \sigma_T\, \frac{L_{iso,\epsilon}}{4\pi\, m_e\, c^3\, R} \\
&> 10^{13} \left(\frac{L_{iso,\epsilon}}{10^{44}\,\text{W}} \right) \left(\frac{t_v}{10\,\text{ms}} \right)^{-1}
\end{aligned} \tag{2}$$

where $n_{ph}(\epsilon)$ is the soft photon number density at energy ϵ and where the pair production cross section has been approximated as the Thomson cross section $\sigma_T = 0.665$ barns (1 barn $= 10^{-28}$ m^2). The opacity in Eq. (2) is huge and would produce a thermal spectrum, in contradiction with the non-thermal power-law spectra observed up to high energies. Considering a source moving at relativistic speed towards the observer can solve this well-known compactness problem. In this case and, e.g., for a pure Band spectrum,[6] the opacity is reduced by a factor $\Gamma^{2(1-\beta)}$, and it can be less than unity for a typical index $\beta \simeq -2.3$ combined with a minimum value of the jet Lorentz factor $\Gamma > \Gamma_{min} \sim 100$ (increasing with E, $1/t_v$, the redshift and the source intensity).

3. GRB observations with Fermi

3.1. The GBM and LAT instruments

Launched in 2008, the Fermi observatory is composed of two instruments that together cover more than seven decades in energy. The Gamma-ray Burst Monitor (GBM; [18]) is comprised of 14 scintillation detectors which monitor the entire sky that is not occulted by the Earth. Spectroscopy with the GBM makes use of 12 NaI detectors between 8 keV and 1 MeV, and of two BGO scintillators which are sensitive to photons of energies between 150 keV and 40 MeV. As a result, the GBM can measure spectra with high time resolution over nearly five decades in energy, covering the low-energy domain where most of the GRB emission takes place [19,20]. At higher energies, the Large Area Telescope (LAT; [21,22]) is a pair-conversion detector sensitive to gamma rays of energies ranging from 20 MeV to more than 300 GeV. The LAT broad energy range,

---

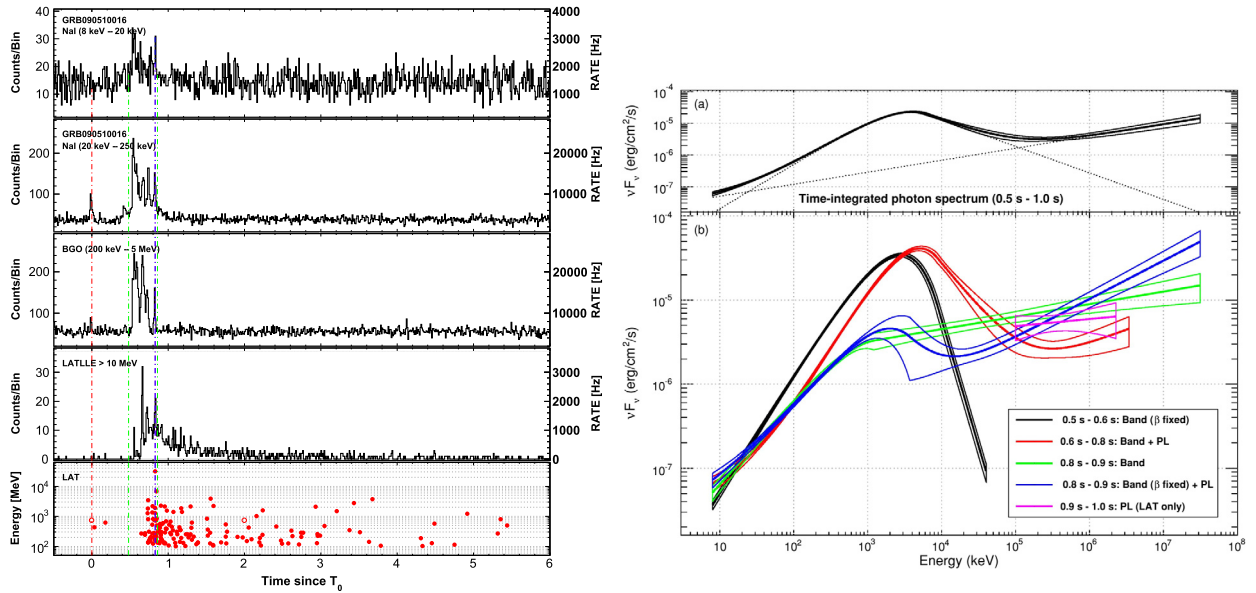[6] See the Supporting Online Material in [17] for a detailed computation.

Fig. 3. Left: GRB 090510 light curves as measured by the Fermi/GBM and the Fermi/LAT [26], from lowest to highest energies: sum of the counts in the GBM NaI detectors (first two panels), in the GBM BGO detector facing the burst (third panel), and in the LAT using all events passing the onboard filter for gamma rays (fourth panel). The last panel displays the energies of the individual photons which are well-reconstructed by the LAT above 100 MeV. Right: GRB 090510 spectral energy distribution (in $\mathrm{erg\,cm^{-2}\,s^{-1}} = 10^{-3}\,\mathrm{W\,m^{-2}}$) as measured by Fermi [27]. Each spectrum is represented by a 68% confidence level contour corresponding to the best fitted spectral shape (i.e. a Band function with an extra power law at high energies).

large effective area ($\sim$0.9 m^2 at peak), low deadtime per event ($\sim$27 μs), wide field of view ($\sim$2.4 sr at 1 GeV) and good angular resolution ($\sim$0.2° at 10 GeV) are vastly improved in comparison with those of its predecessor CGRO/EGRET. They provide more GRB detections and more photons detected from each GRB. Moreover, Fermi was designed with the capability to repoint in the direction of any bright GRB in order to keep its position near the center of the LAT field of view and to observe its afterglow emission during several hours.

The GBM detects 240 bursts per year in average, including 45 short bursts [23,5]. About half of these GRBs occur in the LAT field of view, $\sim$10% of them being detected above 100 MeV. After 6.5 years of operations, the LAT has detected nearly 90 bursts,[7] including seven short bursts. All LAT bright GRBs have benefited from accurate follow-up localizations by the narrow-field instruments onboard Swift [24], facilitating their distance measurement by ground-based optical telescopes. As of today, LAT GRB redshifts range from $z = 0.145$ (GRB 130702A) to $z = 4.35$ (GRB 080916C).

3.2. Some remarkable bursts

The long and bright GRB 080916C is the second LAT-detected burst [17]. Its high-energy emission extended up to 13.2 GeV in the prompt phase, which implied the largest jet Lorentz factor ever measured, $\Gamma_{\min} = 870$. GRB 080916C is also the record holder in terms of energetics, with a source frame energy release[8] $E_{\mathrm{iso}} = 8.8 \times 10^{47}$ J (8.8×10^{54} erg) in the 10 keV–10 GeV energy band, which is equivalent to 4.9 times the Sun's rest mass energy. GRB 080916C prompt emission spectrum features a faint extra power-law component [26]. Its high-energy emission is delayed by a few seconds with respect to its keV–MeV emission and it has been detected up to 1400 s post-trigger, i.e. well after the GBM-detected emission has faded. Subsequent GRB detections with the LAT have revealed that the last two characteristics are common to the vast majority of GRBs at high energies (see section 3.3).

GRB 090510 is the first short and bright burst detected by the LAT [27], with an observed emission extending up to 31.3 GeV in the prompt phase. Its high-energy emission is delayed and temporally extended with respect to its keV–MeV emission (Fig. 3, left). Similarly to all LAT long and bright bursts, its prompt emission spectrum features an extra power-law component. This spectral component dominates the Band function not only at high energies but also below $\sim$20 keV (Fig. 3, right). The afterglow emission of GRB 090510 has been detected by the LAT up to 200 s post-trigger and has been observed

---

[7] http://fermi.gsfc.nasa.gov/ssc/observations/types/grbs/lat_grbs/table.php.

[8] The isotropic equivalent energy is defined as [25] $E_{\mathrm{iso}} = \dfrac{4\pi D_{\mathrm{l}}^2}{1+z} \displaystyle\int_{E_1'/(1+z)}^{E_2'/(1+z)} E\,S(E)\,\mathrm{d}E$, where D_{l} is the luminosity distance, $S(E)$ is the time-integrated

photon spectrum (in $\mathrm{m^{-2}\,keV^{-1}}$) in the observer frame, and $[E_1', E_2']$ is the energy interval in the source frame.
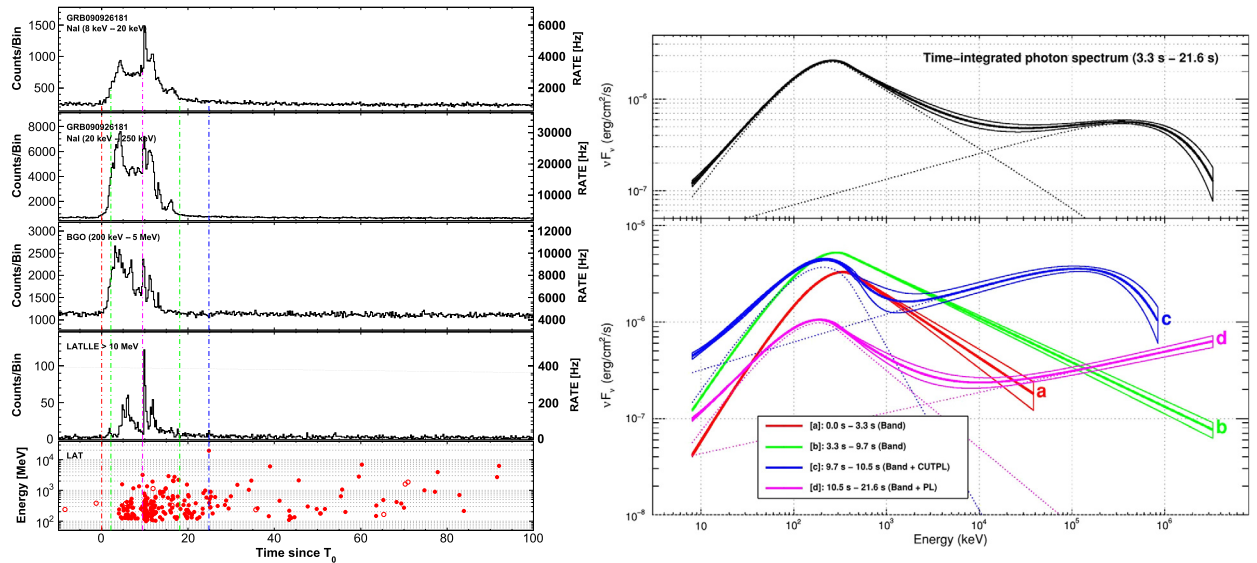
Fig. 4. Left: GRB 090926A light curves as measured by the Fermi/GBM and the Fermi/LAT [26] (see caption of Fig. 3, left). Right: GRB 090926A spectral energy distribution (in erg cm^{-2} s^{-1} = 10^{-3} W m^{-2}) as measured by Fermi [30]. Each spectrum is represented by a 68% confidence level contour corresponding to the best fitted spectral shape (i.e. a Band function with an extra power law at high energies, possibly including a spectral cutoff).

simultaneously by Swift. A forward shock synchrotron emission model (see section 4.2) has been successfully applied to these multi-wavelength observations (from the visible domain to GeV energies) [28].

The high-energy properties of the long and bright GRBs 090902B [29] and 090926A [30] are very similar to those of the two bursts discussed above: presence of an extra power-law component and delayed onset of the high-energy emission, which persisted during 1 ks and 5 ks, respectively. Both temporally extended emissions include multi-GeV photons, e.g., the most energetic event (33.4 GeV) from GRBs 090902B was detected by the LAT 82 s after the GBM trigger. The prompt emission spectrum of GRB 090902B is also peculiar since it contains an important flux in excess to the Band function below ∼50 keV, the origin of which is poorly understood. Moreover, the narrow spectral shape of GRB 090902B around its peak energy E_{p} is difficult to account for in the framework of internal shock synchrotron models (see section 4.2). GRB 090926A is also remarkable, especially for the extreme variability of its prompt light curve. A sharp pulse lasting less than 1 s was observed ∼10 s post-trigger across the whole spectrum (Fig. 4, left). The temporal correlation (within less than 50 ms) between the keV–MeV and GeV prompt emissions during this sharp pulse, which coincides with the emergence of the extra power-law component (Fig. 4, right), suggests that an important fraction of the high-energy emission has an internal shock origin in this case. Moreover, GRB 090926A is unique due to the attenuation of its prompt emission spectrum. The spectral cutoff observed during the sharp pulse (in blue in Fig. 4, right) provided a direct estimate of the jet Lorentz factor Γ (i.e. not just a lower limit as discussed in section 2), ranging from 200 to 700 depending on the $\gamma\gamma$ absorption model which was adopted to solve the compactness problem [30].

GRB 130427A is the brightest burst[9] ever observed by Fermi [31], especially due to its proximity ($z = 0.34$), with more than 500 photons detected by the LAT above 100 MeV, including more than 15 photons above 10 GeV. This burst has also the highest gamma-ray fluence[10] ever (larger than 10^{-6} J m^{-2} = 10^{-3} erg cm^{-2}). The high-energy emission started ∼10 s after the keV–MeV emission, and it includes a 73-GeV photon detected 19 s post-trigger. Unlike other LAT bright GRBs, the high-energy emission of GRB 130427A was very weak in the first instants and thus appeared essentially uncorrelated with its keV–MeV emission (Fig. 5, left). Most importantly, the extra power-law component of GRB 130427A becomes significant only after the end of the GBM-detected emission. As a result, most of the high-energy emission from this burst has been associated with the forward shock in the early afterglow phase [31]. GRB 130427A is also spectacular at later times (Fig. 5, right). It has the brightest afterglow emission ever detected in X rays (though it is not the brightest intrinsically), as well as the longest-lived emission at high energies, which lasted ∼19 h. Very energetic and late gamma rays have been recorded, in particular a 95 GeV photon detected 244 s post-trigger and a 32 GeV photon detected after 34.4 ks. The former is the most energetic photon ever observed from a GRB, and the latter dethrones the 18 GeV photon detected by CGRO/EGRET after 4.5 ks from GRB 940217 (see section 2).

---

[9] The brightness of a burst is defined as the integral of its photon spectrum over time and energy or, equivalently, as the overall number of detected photons.

[10] The fluence of a burst is defined as the integral of its energy flux over time and energy, thus it is indicative of its hardness: $F = T_{90} \int E \frac{\mathrm{d}N}{\mathrm{d}E} \mathrm{d}E$, where T_{90} is the burst duration, usually defined as the interval between the times where the burst has reached 5% and 95% of its total brightness in the same energy range.
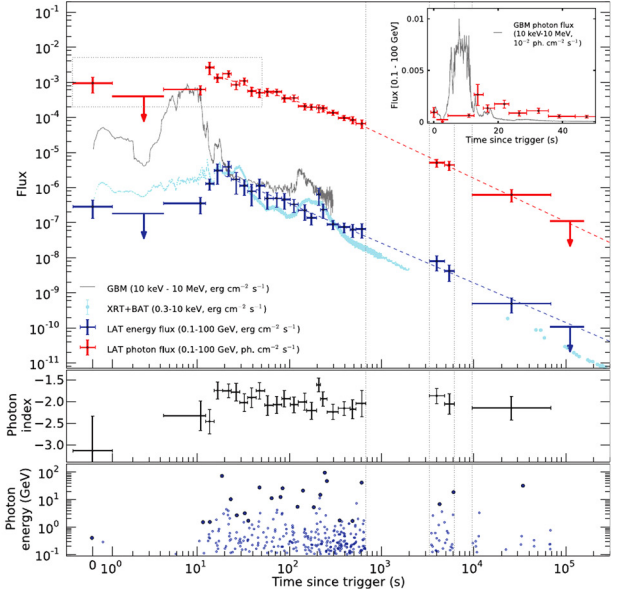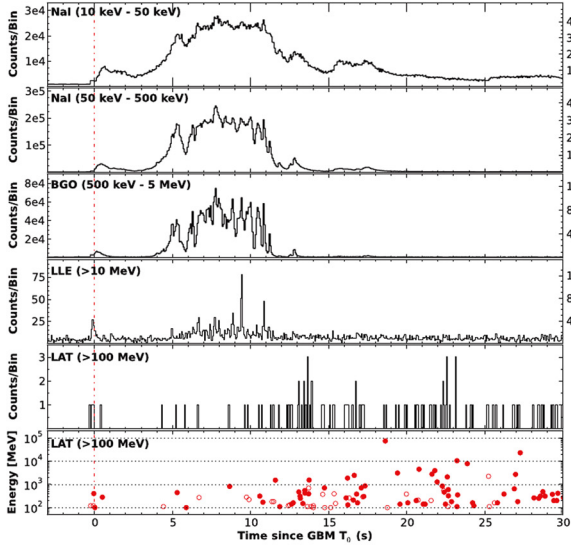
Fig. 5. Left: GRB 130427A light curves as measured by the Fermi/GBM and the Fermi/LAT [31] (see caption of Fig. 3, left). Right: GRB 130427A energy flux light curves (in erg cm^{-2} s^{-1} = 10^{-3} W m^{-2}) as measured by Fermi (GBM and LAT instruments) and Swift (BAT and XRT instruments) [31]. The second panel shows the spectral index α_{EX} of the high-energy power law, and the last panel displays the energies of the individual photons which are well reconstructed by the LAT above 100 MeV.
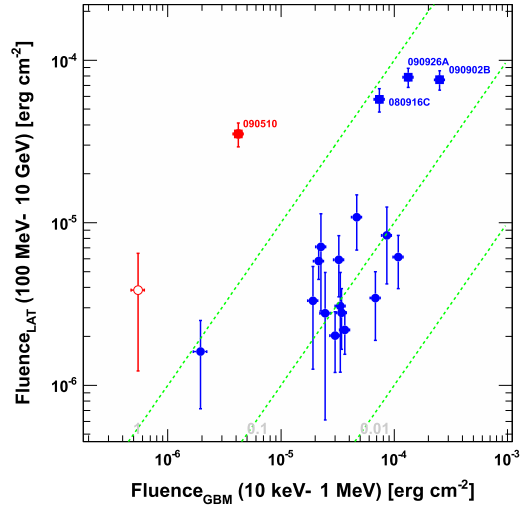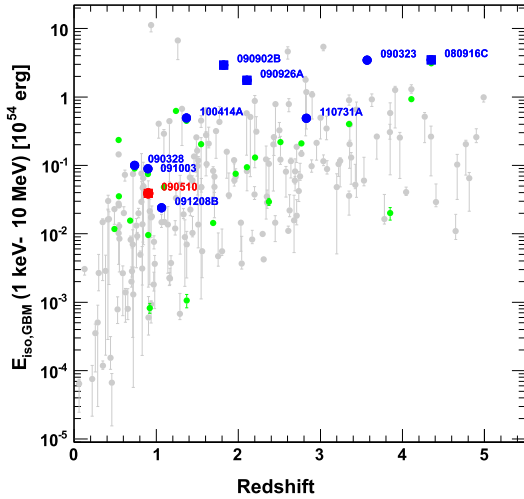

Fig. 6. Left: Isotropic equivalent energy E_{iso} (in erg = 10^{-7} J) in the source frame energy range $[E'_1, E'_2] = [1 \text{ keV}, 10 \text{ MeV}]$ as a function of the redshift for all the GRBs with measured distance in the first Fermi/LAT catalog [26], compared to the GRBs in the Swift/BAT [33] (in gray) and Fermi/GBM [19] (in green) catalogs. Right: Fluence (in erg cm^{-2} = 10^{-3} J m^{-2}) as measured by the Fermi/GBM (10 keV–1 MeV) vs. that measured by the Fermi/LAT (>100 MeV) during their respective T_{90}'s (Fig. 7, right) for all GRBs in the first Fermi/LAT catalog [26]. In both panels, long GRBs are displayed in blue, and short GRBs in red.

3.3. GRB common properties at high energies

The first LAT GRB catalog [26] is a systematic study of GRBs at high energies, covering the first three years of Fermi science operations. Among the 733 GRBs detected by the GBM during this period, the LAT detected 35 bursts including 5 short bursts. Not surprisingly, the LAT-detected GRBs were found to be among the GBM brightest and most fluent GRBs, due to the steepness of the photon spectra and to the LAT limited effective area. The complementary analysis reported in [32] showed that LAT-detected GRBs also have the brightest X-ray luminosities in the afterglow phase (Fig. 8, left). In addition, they are among the most energetic GRBs (intrinsically and observationally), GRB 090510 being the most energetic short one (Fig. 6, left). No particular trend in redshift with respect to the Fermi/GBM and Swift/BAT samples was found. Whereas the fluence in the LAT energy range amounts only to ≈ 10% of the fluence in the GBM energy range for long GRBs, short GRBs
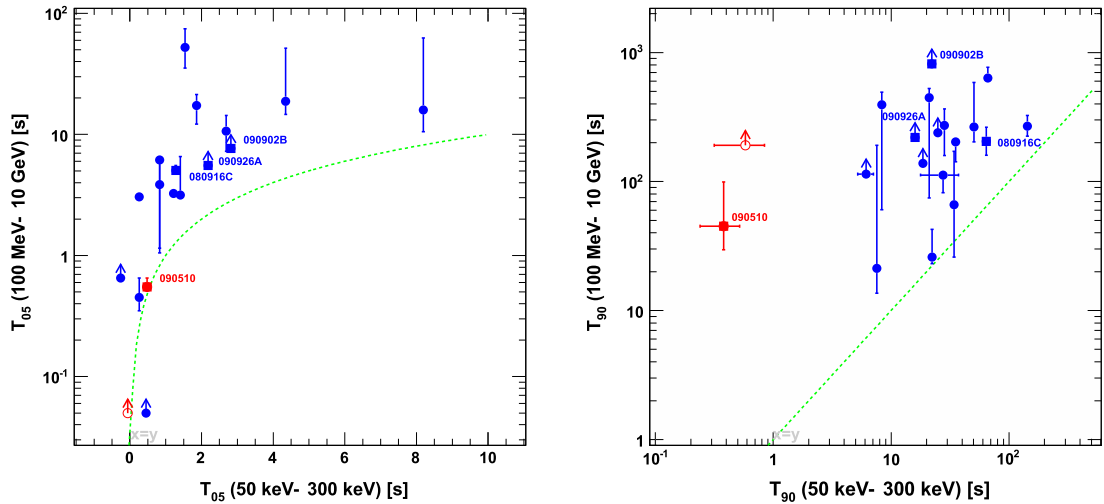
Fig. 7. Onset time (T_{05}, left panel) and duration (T_{90}, right panel) of the GRB emission as measured by the Fermi/GBM (50–300 keV) vs. that measured by the Fermi/LAT (>100 MeV) in the first Fermi/LAT catalog [26]. In both panels, long GRBs are displayed in blue, and short GRBs in red.

seem to have a much larger fluence ratio (Fig. 6, right). Although this result certainly requires more GRB statistics to be firmly confirmed, it suggests different energy outputs above 100 MeV from GRBs depending on their progenitors. Apart from this property, short and long GRBs have shown very similar characteristics in the behavior of their high-energy emission.

The GRB emission detected by the LAT above 100 MeV is systematically delayed with respect to the emission observed with the GBM at keV–MeV energies (Fig. 7, left), and it lasts systematically longer (Fig. 7, right). Specifically, the first pulses in the keV–MeV light curves have no simultaneous counterparts, or only much weaker ones, at high energies, while later pulses can coincide in different energy bands (Figs. 3 and 4, left). In other words, this delay is not caused by an overall shift of the high-energy temporal structures with respect to their potential keV–MeV counterparts.

Joint spectral fits using Fermi GBM and LAT data recorded during the prompt phase showed that the commonly used Band function does not capture all spectral characteristics. Among the 30 GRBs analyzed in [26], this phenomenological shape alone can reproduce the spectrum of 21 GRBs, all other spectra but two (GRBs 090626 and 110721A, for which a logarithmic parabola alone is preferred) are best fitted using either an extra power-law component (GRBs 080916C, 090510, 090902B, 090926A, 100414A and 110731A) and/or an exponential cutoff (GRBs 090926A and 100724B) at high energies. Other deviations from the Band function have been found at lower energies as well. Some GRB spectra contain an important flux in excess to the Band function below ∼50 keV, as reported for GRBs 090510 and 090902B in section 3.2. Moreover, several GRB spectra (e.g., GRBs 100724B, 110721A and 120323A) exhibit a shoulder on top of the low-energy branch of the Band function, which has been interpreted [34–36] as the jet thermal emission expected at the photospheric radius ($R_{ph} \approx 10^{9-10}$ m, where the jet plasma becomes transparent to its own radiation) [37]. These examples illustrate the GRB spectral diversity in their prompt emission phase, and clearly call for the development of detailed broad-band physical models as a prerequisite to understanding GRB emission at the highest energies (see section 4.2).

At late times, the GRB high-energy emission looks simpler and its origin seems less unclear. After the end of the keV–MeV prompt emission, no noticeable spectral evolution is observed, the photon spectrum is well reproduced by a single power-law component of index $\alpha_{EX} \simeq -2$ (see, e.g., the second panel of Fig. 5, right), and the luminosity decays smoothly (Fig. 8, right). As discussed in section 4.2, such a decay phase is consistent with a forward shock origin of the high-energy emission during the afterglow phase. Specifically, the high-energy luminosity decays as $L(t) \propto t^\delta$ with $\delta \simeq -1$ for all GRBs but three (GRBs 090510, 090902B and 090926A), for which a broken power law is detected [26]. For these bursts, the time of the break is observed after the end of the keV–MeV emission as measured by the GBM, and δ switches from ≈ -2 to -1. Defining the decay index δ_∞ as the value of δ at very late times, all GRBs[11] thus follow a unique power-law decay with $\delta_\infty \simeq -1$.

4. Physical implications and discussion

4.1. Constraints on GRB jet Lorentz factors

The Fermi/LAT has detected high-energy emission without any spectral attenuation beyond a few (tens of) GeV from several bright GRBs [17,27,29,30]. Setting the gamma-ray opacity to pair production to unity in Eq. (2), the highest-energy

---

[11] Except GRBs 080916C and 110731A. However, these long GRBs have the shortest intrinsic durations at high energies, suggesting that a non-detected temporal break could still be present at later times.
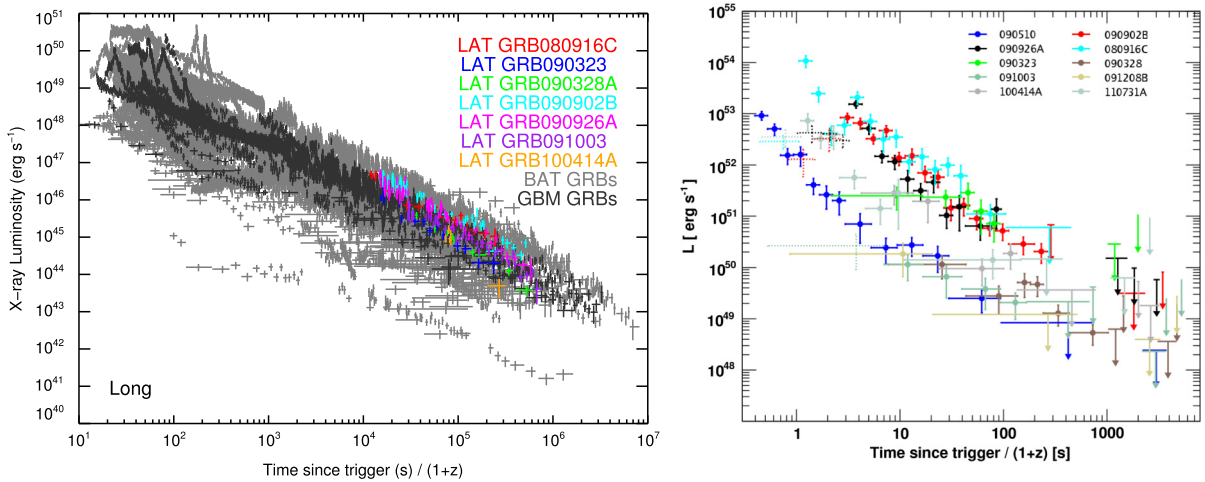
Fig. 8. Left: Decay of the X-ray (0.3–10 keV) luminosity (in erg s^{-1} = 10^{-7} W) with time measured in the source frame for two samples of GRBs detected by Swift (in gray) and Fermi/LAT (in color) [33]. Right: Decay of the high-energy (>100 MeV) luminosity (in erg s^{-1} = 10^{-7} W) with time measured in the source frame for all the GRBs with known redshift and detected extended emission in the first Fermi/LAT catalog [26].

detected photons provided lower limits $\Gamma_{min} \approx 1000$ on the jet Lorentz factor (Fig. 9, left), revealing that both long and short GRBs can have high outflow velocity, a key result for GRB modeling. It must be noted that the identification of the soft photons responsible for the $\gamma\gamma$ absorption is a delicate task, and ideally requires spectroscopy with good statistics over the considered variability time scale t_v (see Eq. (2)). In practice, t_v is chosen as the fastest variability observed in the Fermi/GBM light curve (e.g., 50 ms for GRB 090902B, while some variability is observed in the LAT down to ∼90 ms [29]), and the target photon spectrum is derived over slightly larger durations. Moreover, the target photon field is considered uniform, isotropic and time-independent in this simple one-zone steady-state model. More realistic computations [38,39], which account for geometrical and dynamical effects, can lead to smaller opacities and thus to Γ_{min} values which are 2 to 3 times smaller.

Whereas ∼9.3 LAT-detected GRBs with more than 10 photons above 100 MeV were expected per year from pre-launch estimates [40], a mean rate of ∼6.3 GRBs per year was obtained in the first Fermi/LAT catalog [26]. The past estimates were possibly affected by systematic uncertainties, e.g., arising from the extrapolations from the CGRO/BATSE energy range to the LAT energy range, which are uncertain due to the large lever arm combined with the errors ϵ_β in measuring the Band function index β. However, the lack of LAT GRB detections raises the question whether the high-energy emission is suppressed and if spectral cutoffs are more common than anticipated, similarly to the attenuated spectrum of GRB 090926A (Fig. 4, right). Such cutoffs should be even more pronounced and affect the observed spectra above a few tens of MeV in order to completely turn off the high-energy emission and to prevent any high-energy component from emerging in the LAT energy range.

In order to investigate this question, a list of LAT non-detected GRBs which were bright and/or spectrally hard in the GBM energy domain has been extracted from a sample of 288 GRBs detected by the GBM during the first 2.5 years of Fermi science operations [41]. Among the 30 GRBs with more than 70 counts/s in the GBM BGO detectors and with a good measurement of the Band function index β ($\epsilon_\beta < 0.5$), 6 GRBs require a degree of spectral softening between the BGO and the LAT energy ranges to explain their LAT non-detection. The flux and hardness (E_P and β, see Eq. (1)) of these GRBs are representative of the initial sample. However, they have the smallest ϵ_β values, indicating that a very accurate spectroscopy is required to reveal the spectral feature. Assuming that this softening is due to gamma-ray opacity to pair production, upper limits Γ_{max} ranging from 150 to 650 were derived for the jet Lorentz factors of these GRBs, using a similar formalism as in Eq. (2) with a conservative $t_v = 100$ ms variability time scale. As a result, the comparison of these limits to previous constraints on Γ suggests that GRBs span a relatively broad range of jet velocities (Fig. 9, left).

4.2. Possible origins of the GRB emission at high energies

4.2.1. Emissions of internal origin

From an observational point of view, the GRB prompt phase can be reasonably defined as the period of time where the keV–MeV emission consists of impulsive and pulsed structures. This definition might be too simplistic since it relies on durations (i.e. T_{90}'s) obtained with background-limited detectors such as the Fermi/GBM, but I will adopt it in the following discussion. The GRB prompt emission in the keV–MeV domain is often attributed to the synchrotron emission of internal-shock accelerated electrons. At low energies, the synchrotron model predicts a spectral index value between $-3/2$ (for electrons in a fast-cooling regime) and $-2/3$ (in a slow cooling regime) [42], whereas the observed Band function index α is distributed around -1. The GRB extreme variability and brightness imply efficient radiative processes and suggest that
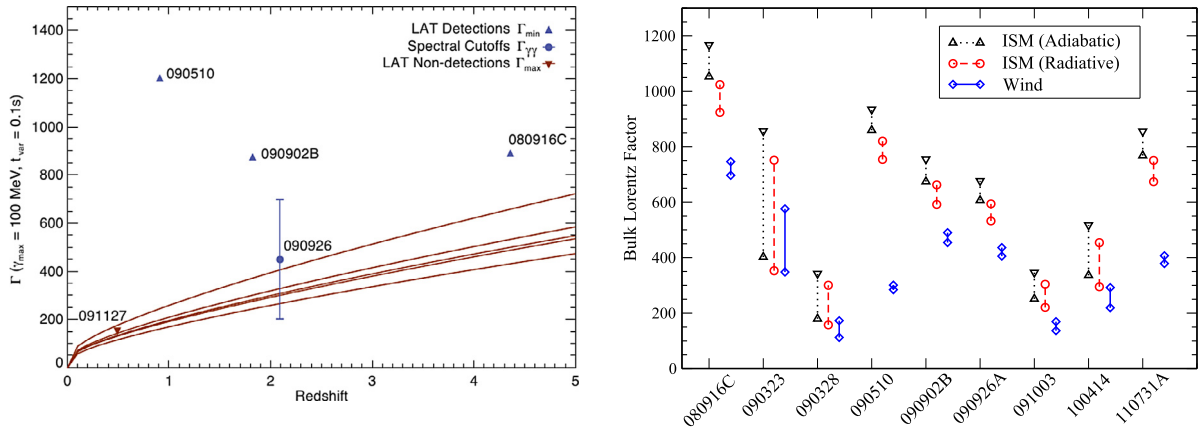
Fig. 9. Constraints from Fermi on GRB jet Lorentz factors. Left: Curves giving upper limits Γ_{max} on the jet Lorentz factors as a function of the redshift for 6 GRBs exhibiting a spectral softening at a few tens of MeV [41]: GRBs 080925, 081207, 090131, 090528B, 100724B, and 091127. The latter burst has a known redshift and is shown with a brown triangle. Lower limits Γ_{min} (GRBs 080916C, 090510, 090902B) and measurement (GRB 090926A) for Fermi/LAT bright GRBs are superimposed (blue triangles and point, respectively). The target photon field for $\gamma\gamma$ absorption is assumed uniform, isotropic and time-independent, but the error bar for GRB 090926A accounts for different models [30], illustrating the overall scaling that could be applied to the entire figure. Right: Jet Lorentz factor for all the GRBs with known redshift in the first Fermi/LAT catalog [26]. These estimates assume that the high-energy peak flux time marks the start of the jet deceleration by the circum-burst medium (inter-stellar medium with uniform density or massive star wind, which is more appropriate for long GRBs).

the slow-cooling regime is not suitable. Anyhow, many GRBs have shown to be hard enough at low energies for their Band function index α to exceed the limit in this regime as well [43]. Since this so-called line-of-death problem challenges the internal shock synchrotron model, several theoretical extensions have been recently proposed which predict, e.g., an increase of the spectral index caused by the retreatment of low-energy photons through inverse Compton processes [44] or by the presence of an additional thermal component [34–36], or a pure thermal emission in extreme cases like GRB 090902B [45].

At high energies, two different classes of models consider the emission of internal-shock accelerated particles in order to explain the extra power-law component observed in the prompt phase of Fermi/LAT bright GRBs (a priori, these models do not address the temporal extension of the high-energy emission). So-called leptonic models are based on electron syn-chrotron emission at keV–MeV energies and inverse Compton or SSC processes at high energies. They naturally predict the fast variability observed in GRB light curves, and the temporal correlation between different energy bands, similarly to the sharp pulse of GRB 090926A. However, this first class of models needs some fine tuning (see, e.g., [46]) to produce a delayed onset of the high-energy emission that is longer than the spike widths, each pulse in the light curve marking a different shell collision and shock. Such models also have difficulties to produce the flux excess which is sometimes observed below $\sim$50 keV (Fig. 3, right). This flux excess is indeed compatible with the extension to the lowest energies of the high-energy extra power-law component, which is not expected from inverse Compton processes.

So-called hadronic models, which form the second class of models, investigate GRBs as possible sources of the ultra-high energy cosmic rays [47] (of energies greater than 1 EeV = 10^{18} eV).[12] In the high-energy gamma-ray domain, hadronic models consider the proton synchrotron emission [49,50] and/or the inverse Compton emission from secondary e^+e^- pairs produced in internal cascades initiated by accelerated protons or ions (through $p + \gamma \rightarrow p/n + \pi^0/\pi^+$ processes) [51]. In these models, the delayed onset of the high-energy emission could result from the time needed to accelerate protons and ions and to develop cascades, but these models do not naturally predict the aforementioned correlated variability and have difficulties to produce high-energy pulses with similar width as the keV–MeV pulses. While synchrotron emission from secondary e^+e^- pairs could explain the flux excess below $\sim$50 keV, these models require an energy injected in the magnetic fields or in the protons which is 10^{2-3} larger than observed. It must be noted that in the proton synchrotron model, this constraint strongly depends on the jet Lorentz factor ($\propto \Gamma^{16/3}$, see [49]) and could be accommodated with low values of this key parameter similar to those discussed in section 4.1.

4.2.2. Emissions of external origin

An alternative interpretation of GRB properties at high energies, which is nevertheless also not fully satisfactory, is provided by the early and late afterglow models. Unlike the internal shock models discussed above, these models consider the synchrotron emission from electrons accelerated at the forward shock, which is produced by the interaction of the jet with the circum-burst medium.

---

[12] The secondary neutrino emission implied by hadronic models is potentially detectable by future experiments such as IceCube (http://icecube.wisc.edu) and KM3NeT (http://www.km3net.org/home.php). GRBs are thus good source candidates for the develop-ment of multi-messenger astrophysics in the coming years and for the advance of high-energy neutrino astronomy, which is still in its infancy [48].
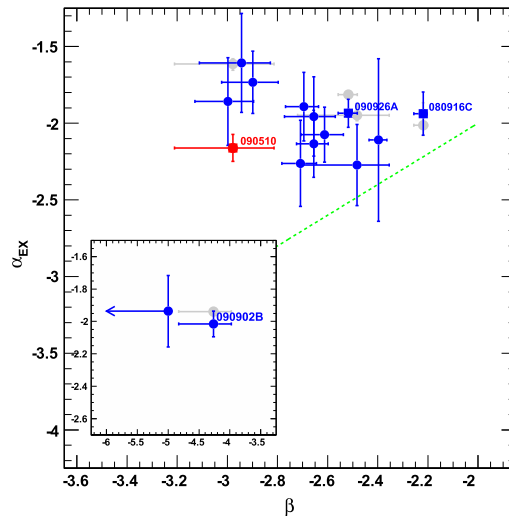
Fig. 10. Comparison, for all the GRBs analyzed in the first Fermi/LAT catalog [26], of the Band function index β with the spectral index α_{EX} of the high-energy power-law component. Values displayed in color (blue for long GRBs and red for the short GRB 090510) were obtained from a power-law spectral fit (yielding α_{EX}) to the LAT data recorded after the end of the GBM-detected emission, and from a Band spectral fit (yielding β) to the GBM and LAT data recorded during the period of the GBM-detected emission (T_{90}). If, in the latter case, the data require an extra power law beyond the Band function at high energies, then both fitted indices are indicated in gray.

The smooth decay of the high-energy luminosity at late times (see section 3.3 and Fig. 8, right) is similar to the behavior of the visible/UV and X-ray emission in the afterglow phase (Fig. 8, left). In addition, Fig. 10 shows that the spectral index α_{EX} of the extra power-law component is clustered around -2, either after the end of the keV–MeV emission (points in color in the figure; see also the second panel of Fig. 5, right) or during the prompt phase of Fermi/LAT bright GRBs (gray points; see also Figs. 3 and 4, right). This stability of the high-energy spectrum contrasts with the spectral variability of the keV–MeV emission, as shown in Fig. 10 by the different values of the Band function index β. Finally, β is systematically lower than α_{EX}. These findings suggest that the high-energy emission results essentially from a mechanism which is independent from internal shocks, namely from the forward shock. Furthermore, they indicate that the forward shock high-energy emission not only accounts for the luminosity observed during the late afterglow phase, and that it can also be dominant while the prompt keV–MeV emission from internal shocks remains detectable. It must be stressed, however, that the high-energy contribution from internal shocks is still required during highly variable episodes in the prompt phase, as in the case of the sharp pulse of GRB 090926A. Distangling both contributions may be possible in the future through time-resolved spectral analyses of Fermi data which combine spectroscopy with a full characterization of the variability properties at high energies. Future LAT-detected bursts similar to GRBs 090510, 090902B and 090926A would be also helpful, since the initial steep decay ($\delta \approx -2$) observed in their high-energy light curves may mark the transition from a phase where the forward shock emission is contaminated or even dominated by the prompt high-energy emission, to a pure afterglow phase.

The forward shock synchrotron emission models have been successfully applied to the Swift and Fermi multi-wavelength observations of the afterglow phase of GRBs 090510 and 110731A [28,52–54]. These models predict a relation between the luminosity decay index δ and the spectral index α_{EX}, which depends on the considered energy range. Above 100 MeV, electrons are in a fast-cooling regime and radiate efficiently. In this case, the relation takes the form $\delta = (14 + 12\,\alpha_{EX})/7 \simeq -10/7$ for a blast wave expansion where radiative losses are important, and $\delta = (4 + 3\,\alpha_{EX})/2 \simeq -1$ for an adiabatic expansion [42,55]. The latter case is clearly favored by the decay index $\delta_\infty \simeq -1$ measured by the Fermi/LAT at very late times (see also [50,56,57]).

The forward shock synchrotron emission models can also explain the delayed onset of the high-energy emission, which is attributed to the time required for the flux to increase during the early afterglow phase until it becomes detectable by the Fermi/LAT [28,50,56,58]. The high-energy flux increases as t^2 due to the progressive energy dissipation which results from the jet deceleration by the circum-burst medium. After the peak flux time, the outflow slows down considerably and reaches non-relativistic velocities [59,60]. Estimates of the jet Lorentz factor Γ can be obtained from the observation of the early afterglow phase, assuming that the peak flux time which is measured by the LAT above 100 MeV is of the order of the jet deceleration time. These estimates are thus larger for smaller delays, and they range from 200 to 1000 (Fig. 9, right) for all the GRBs with known redshift in the first Fermi/LAT catalog [26]. These values are compatible with those obtained from opacity arguments (see section 4.1), and they provide an independent confirmation that both long and short GRBs have relativistic outflows.

Afterglow models can be further explored at high energies by comparing the most energetic photons detected by the Fermi/LAT with the maximum synchrotron photon energy, $E_{syn,max}$. Assuming a single acceleration and emission region, this energy can be derived by equating the electron acceleration time scale, t_{acc}, and the electron energy loss time scale due to synchrotron radiation. The acceleration time scale can be approximated as the inverse of the Larmor angular frequency
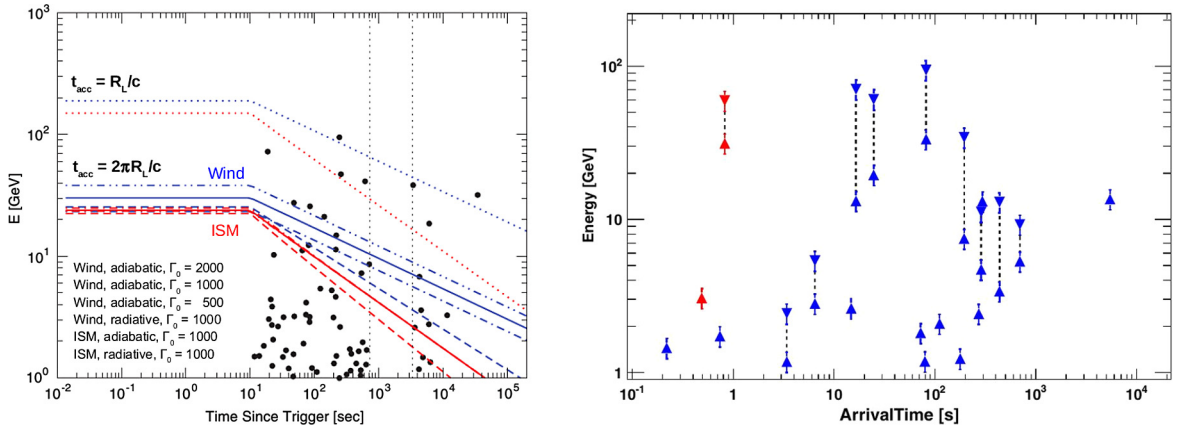
Fig. 11. Left: Maximum synchrotron energy in the forward shock model for GRB 130427A as a function of time [31]. Line styles denote different hypotheses regarding the initial value of the jet Lorentz factor and the structure of the circum-burst medium (inter-stellar medium with uniform density or massive star wind, which is more appropriate for long GRBs). Black dots indicate the high-energy photons detected by the Fermi/LAT. Right: Observed (upward-pointing triangles) and source frame (downward-pointing triangles) energy and arrival time for the highest-energy photons associated with the long (blue) and short (red) GRBs in the first Fermi/LAT catalog [26].
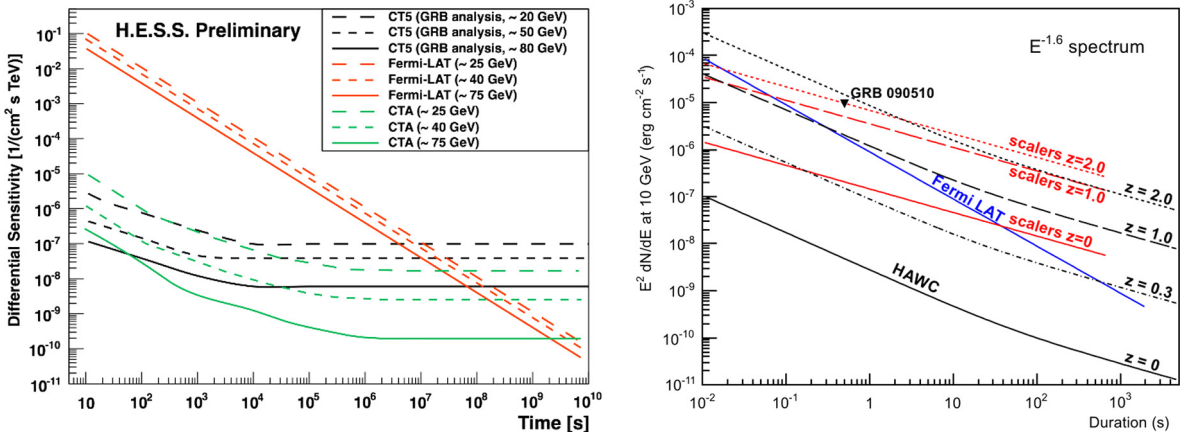

Fig. 12. Sensitivity to transient sources of very high-energy telescopes (HESS CT5 and CTA, left panel; HAWC, right panel) as a function of the signal duration, for various energy thresholds (left panel) and redshifts (right panel), as compared to the Fermi/LAT. CTA curves correspond to an analysis which has been optimized for GRB and pulsar studies [68]. HAWC curves (in $\mathrm{erg\,cm^{-2}\,s^{-1}} = 10^{-3}\,\mathrm{W\,m^{-2}}$) correspond to a 20° zenith angle of the observed source, and account for the absorption of high-energy gamma rays by the Extra-galactic Background Light [70].

($t_{acc} \simeq R_L/c$, which corresponds to an extremely fast acceleration) or as the Larmor time scale for an electron to execute a gyration ($t_{acc} \simeq 2\pi R_L/c$, more realistic) [61]. In the case of GRB 130427A, this yields a conservative limit $E_{syn,max}(t) \approx 80\,\Gamma(t)$ MeV [31]. As shown in the left panel of Fig. 11, this limit is violated by several LAT-detected photons. In particular, the 95 GeV photon detected after 244 s and the 32 GeV photon detected after 34.4 ks are clearly incompatible with a synchrotron origin. Although an SSC interpretation has been considered by several authors [62,63], this scenario is not favored by the absence of an inverse Compton spectral component in the LAT energy range [31], which is reinforced by joint detections with the *NuSTAR* X-ray satellite after 1.5 and 5 days [64], and by flux upper limits from the VERITAS Cherenkov telescopes in the very high-energy range after 1 day [65]. Fermi/LAT observations of GRB 130427A therefore challenge the forward shock synchrotron emission models in their simplest version, and they call at least for a better description of external shock micro-physics.

5. Prospects for GRB observation at very high energies

The observation by the Fermi/LAT of several GRB photons with energies reaching 10–100 GeV in the source frame (Fig. 11, right), as late as ~1 day after the trigger in the case of GRB 130427A (Fig. 11, left), is an encouraging sign for GRB detections at very high energies with ground-based experiments, either with arrays of imaging atmospheric Cherenkov
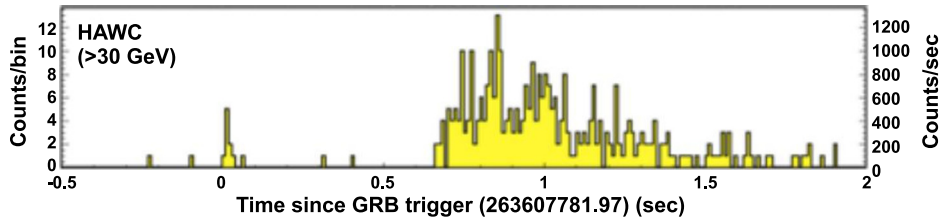
Fig. 13. HAWC simulation of GRB 090510 light curve above 30 GeV, obtained by extrapolating the Fermi/LAT spectrum to very high energies and including the effect of gamma-ray absorption by the Extra-galactic Background Light [69].

telescopes (IACTs) such as HESS[13], MAGIC[14], VERITAS[15] and the future CTA observatory[16] [66], or with synoptic detectors such as HAWC[17] and LHAASO.[18] These experiments (see [67] for more details) try to achieve low energy thresholds, ideally as low as ~10 GeV in order to limit the absorption of high-energy gamma rays from distant sources by the Extra-galactic Background Light. Due to their huge effective area (of a few hectares, typically), they can accumulate large photon statistics and their sensitivity to transient sources can surpass the Fermi/LAT sensitivity beyond 10–100 GeV (Fig. 12).

Observations of GRBs with IACTs have always led to upper limits so far, on time scales ranging from a few tens of seconds to days. Apart from the faintness of most GRBs at very high energies, the reasons for this lack of success include the relatively high energy threshold (~100–200 GeV) of past experiments, a low duty cycle (~10%), as well as the combination of the IACT narrow field of view (a few degrees) with the poor localization capabilities of the most productive space detectors (e.g., the CGRO/BATSE and the Fermi/GBM) and with the time needed to repoint and start follow-up observations. Synoptic detectors have ~1 sr fields of view and a $\lesssim$100% duty cycle, yet higher energy thresholds and lower sensitivities than IACTs, due to their smaller power in rejecting the background events induced by charged cosmic rays. As a result, the response time and sensitivity of IACTs and synoptic detectors match adequately the time scales and brightness of long and short GRBs, respectively. As an example, Fig. 13 shows a simulation of the light curve that HAWC would have recorded above 30 GeV from the short GRB 090510 if the experiment had been operational in 2009.

Extrapolating Fermi/LAT GRB spectra to the very high-energy range is difficult, in particular it remains unclear whether the extra power-law component observed in the spectra of several bright GRBs is a common property at GeV energies. In addition, intrinsic spectral cutoffs similar to the case of GRB 090926A are expected at 1–100 GeV energies, and they are strongly related to the value of the jet Lorentz factor whose distribution among GRBs is not precisely known. For these reasons, current estimates of GRB detection rates at very high energies suffer from important uncertainties and amount to ≈ 1 GRB per year depending on the considered experiment [70–73]. During the coming years, a few but invaluable GRB detections are thus expected beyond 10–100 GeV. As VERITAS and HAWC upper limits on GRB 130427A emission already suggest [65,74], future detections at very high energies will provide new constraints on GRB jet physics and useful information regarding their acceleration and emission processes at the highest energies.

6. Conclusions

Since its launch in 2008, the Fermi Gamma-ray Space Telescope has made important breakthroughs in the understanding of the GRB phenomenon. The combination of the Fermi GBM and LAT instruments provided high quality data over seven decades in energy for a large sample of GRBs, and it made GRB population studies possible at high energies. It revealed that both short and long GRBs have relativistic outflows and share similar properties. Their emission above 100 MeV is delayed and temporally extended with respect to the emission detected at keV–MeV energies. While the origin of the delayed onset remains unclear, the long-lived GeV emission is consistent with the afterglow emission of a blast wave in adiabatic expansion, as confirmed by the stability of its spectrum which contrasts with the spectral variability of the prompt keV–MeV emission. However, high-energy observations of GRB 130427A put severe constraints on forward shock synchrotron emission models. Understanding the complex GRB spectral evolution during their prompt emission phase also requires new theoretical developments and detections of more and brighter GRBs in the future, accompanied by more detailed time-resolved spectroscopy, in order to pinpoint which high-energy processes dominate throughout the GRB. In particular, the connection between the extra power-law component seen by the LAT at high energies in the prompt phase and the long-lived GeV emission observed up to several (tens of) kilo-seconds, is of great importance in understanding the transition from the internal shock phase to the early and late afterglow phases.

The Fermi and Swift observatories have provided (and still provide) a good characterization of GRB prompt and afterglow emissions, respectively. In the future, SVOM [75] panchromatic observations from the near infra-red domain to MeV

energies will bring new spectro-temporal diagnosis during the entire period of activity of each GRB, from the prompt phase (and possible precursors) to the late afterglow phase. Scheduled for a launch in 2021, the SVOM mission will thus provide a broad view of the GRB phenomenon, which will be completed at higher energies by new space-based gamma-ray observatories [67] and, in a few cases, by observations with ground-based facilities such as CTA and HAWC.

References

[1] T. Piran, Rev. Mod. Phys. 76 (2004) 1143.
[2] E. Nakar, Phys. Rep. 442 (2007) 166.
[3] G. Vedrenne, J.-L. Atteia, Gamma-Ray Bursts: The Brightest Explosions in the Universe, Springer & Praxis Publishing, 2009.
[4] C. Kouveliotou, et al., Astrophys. J. Lett. 413 (1993) 101.
[5] A. Von Kienlin, et al., Astrophys. J. Suppl. Ser. 211 (2014) 13.
[6] J. Abadie, et al., Astrophys. J. 760 (2012) 12.
[7] P. Kumar, B. Zhang, Phys. Rep. 561 (2014) 1.
[8] F. Piron, V. Connaughton, The Fermi view of gamma-ray bursts, C. R. Physique 12 (2011) 267.
[9] D. Horns, A. Jacholkowska, C. R. Physique 17 (6) (2016) 632–648, in this issue.
[10] D. Band, et al., Astrophys. J. 413 (1993) 281.
[11] M.S. Briggs, et al., Astrophys. J. 524 (1999) 82.
[12] M.M. Gonzalez, et al., Nature 424 (2003) 749.
[13] A. Giuliani, et al., Astron. Astrophys. 491 (2008) L25.
[14] M. Sommer, et al., Astrophys. J. Lett. 422 (1994) L63.
[15] J. Granot, et al., Astrophys. J. Lett. 598 (2003) L11.
[16] K. Hurley, et al., Nature 372 (1994) 652.
[17] A.A. Abdo, et al., Science 323 (2009) 1688.
[18] C. Meegan, et al., Astrophys. J. 702 (2009) 791.
[19] A. Goldstein, et al., Astrophys. J. Suppl. Ser. 199 (2012) 19.
[20] D. Gruber, et al., Astrophys. J. Suppl. Ser. 211 (2014) 12.
[21] W.B. Atwood, et al., Astrophys. J. 697 (2009) 1071.
[22] D.J. Thompson, C. R. Physique 16 (2015) 600.
[23] B. Paciesas, et al., Astrophys. J. Suppl. Ser. 199 (2012) 18.
[24] N. Gehrels, et al., Astrophys. J. 611 (2004) 1005.
[25] G. Ghirlanda, et al., Astrophys. J. 616 (2004) 331.
[26] M. Ackermann, et al., Astrophys. J. Suppl. Ser. 209 (2013) 11.
[27] A.A. Abdo, et al., Astrophys. J. 716 (2010) 1178.
[28] M. de Pasquale, et al., Astrophys. J. Lett. 709 (2010) L146.
[29] A.A. Abdo, et al., Astrophys. J. Lett. 706 (2009) L138.
[30] A.A. Abdo, et al., Astrophys. J. 729 (2011) 114.
[31] M. Ackermann, et al., Science 343 (2014) 42.
[32] N.R. Butler, et al., Astrophys. J. 671 (2007) 656.
[33] J.L. Racusin, et al., Astrophys. J. 738 (2011) 138.
[34] S. Guiriec, et al., Astrophys. J. Lett. 727 (2011) L33.
[35] M. Axelsson, et al., Astrophys. J. Lett. 757 (2011) L31.
[36] S. Guiriec, et al., Astrophys. J. 770 (2013) 32.
[37] F. Daigne, R. Mochkovitch, arXiv:astro-ph/0303288, 2003.
[38] J. Granot, et al., Astrophys. J. 677 (2008) 92.
[39] R. Hascoët, et al., Mon. Not. R. Astron. Soc. 421 (2012) 525.
[40] D.L. Band, et al., Astrophys. J. 701 (2009) 1673.
[41] M. Ackermann, et al., Astrophys. J. 754 (2012) 121.
[42] R. Sari, et al., Astrophys. J. Lett. 497 (1998) L17.
[43] R.D. Preece, et al., Astrophys. J. Lett. 506 (1998) L23.
[44] F. Daigne, et al., Astron. Astrophys. 526 (2011) 110.
[45] F. Ryde, et al., Astrophys. J. Lett. 709 (2010) L172.
[46] Z. Bosnjak, et al., Astron. Astrophys. 498 (2009) 677.
[47] M. Vietri, Astrophys. J. 453 (1995) 883.
[48] M.G. Aartsen, et al., Science 342 (2013) 947.
[49] S. Razzaque, et al., Open Astron. J. 3 (2010) 150.
[50] S. Razzaque, Astrophys. J. Lett. 724 (2010) L109.
[51] K. Asano, et al., Astrophys. J. Lett. 705 (2009) L191.
[52] M. Ackermann, et al., Astrophys. J. 763 (2013) 71.
[53] M. Lemoine, et al., Mon. Not. R. Astron. Soc. 435 (2013) 3009.
[54] X.-Y. Wang, et al., Astrophys. J. Lett. 771 (2013) L33.
[55] J. Granot, R. Sari, Astrophys. J. 568 (2002) 820.
[56] P. Kumar, R. Barniol Duran, Mon. Not. R. Astron. Soc. 409 (2010) 226.
[57] L. Nava, et al., Mon. Not. R. Astron. Soc. 443 (2014) 3578.
[58] G. Ghisellini, et al., Mon. Not. R. Astron. Soc. 403 (2010) 926.
[59] R.D. Blandford, C.F. McKee, Phys. Fluids 19 (1976) 1130.
[60] R. Sari, Astrophys. J. Lett. 489 (1997) L37.
[61] M. Lemoine, G. Pelletier, C. R. Physique 16 (2015) 628.
[62] R.-Y. Liu, et al., Astrophys. J. Lett. 773 (2013) L20.
[63] Y.-Z. Fan, et al., Astrophys. J. 776 (2013) 95.
[64] C. Kouveliotou, et al., Astrophys. J. Lett. 779 (2013) L1.
[65] E. Aliu, et al., Astrophys. J. Lett. 795 (2014) L3.
[66] M. Actis, et al., CTA Consortium, Exp. Astron. 32 (2011) 193.

[67] J. Knödlseder, C. R. Physique 17 (6) (2016) 663–678, in this issue.
[68] C. Stegmann, et al., in: Proc. Astroparticle Physics 2014, Amsterdam, June 2014, http://indico.cern.ch/event/278032/session/9/contribution/226.
[69] K. Tollefson, et al., http://moriond.in2p3.fr/J13/program.php, 2013.
[70] A.U. Abeysekara, et al., Astropart. Phys. 35 (2012) 641.
[71] S. Inoue, et al., Astropart. Phys. 43 (2013) 252.
[72] R.C. Gilmore, et al., Exp. Astron. 35 (2013) 413.
[73] I. Taboada, et al., Nucl. Instrum. Methods A 742 (2014) 276.
[74] A.U. Abeysekara, et al., Astrophys. J. 800 (2015) 78.
[75] J. Paul, et al., C. R. Physique 12 (2011) 298, arXiv:1104.0606 [astro-ph.HE].